Supplemental Figures

Anti-EGFR Affibodies with Site-Specific Photocrosslinker Incorporation Show Both Directed Target-Specific Photoconjugation and Increased Retention in Tumors

Michael Brasino,[1] Shambojit Roy,[1] Annette H. Erbse,[2] Liangcan He,[1] Chenchen Mao,[3] Wounjhang Park,[3,4] Jennifer N. Cha*[1,4] and Andrew P. Goodwin*[1,4]

[1]Department of Chemical and Biological Engineering, [2]Department of Chemistry and Biochemistry, [3]Department of Electrical, Computer, and Energy Engineering, and [4]Materials Science and Engineering Program, University of Colorado, 596 UCB, Boulder, CO, 80303.

*To whom correspondence should be addressed: Jennifer.Cha@colorado.edu, Andrew.Goodwin@colorado.edu

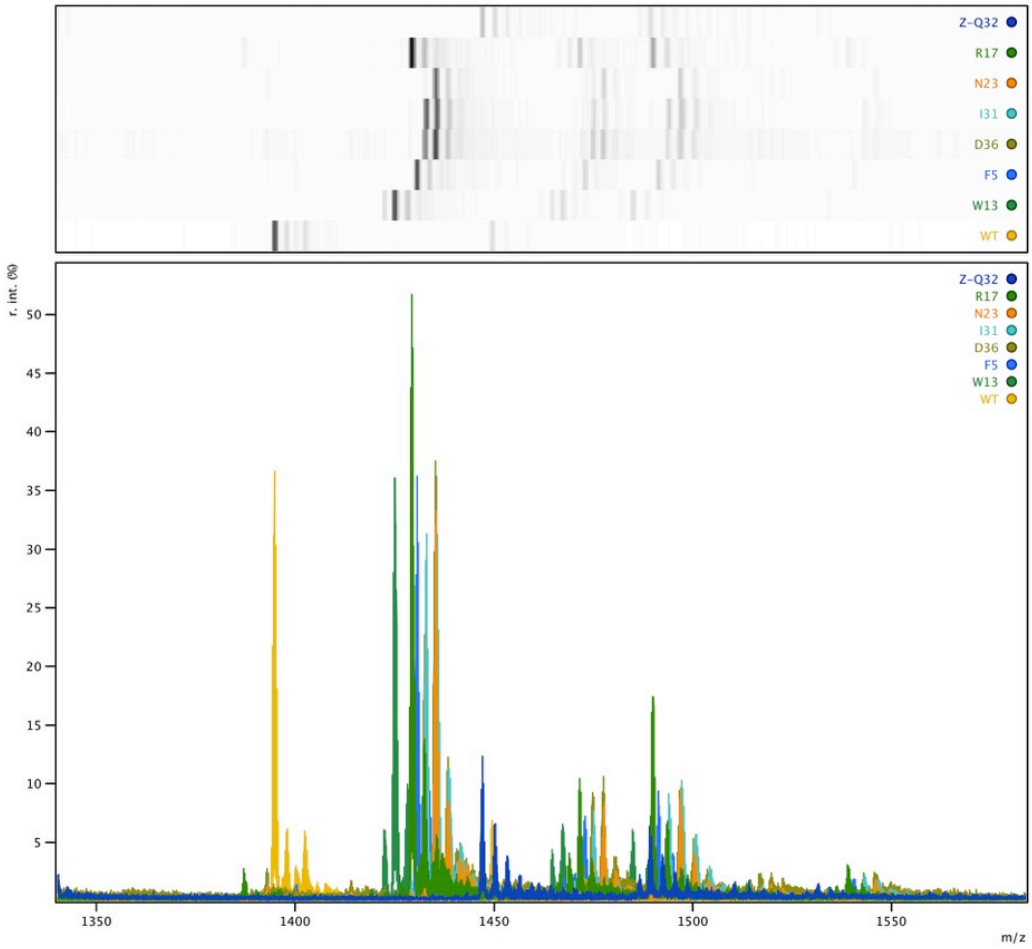

Figure S1: Electron Spray Ionization MS spectra of EGFR binding affibody ZEGFR:1907 (WT) compared to mutants containing cysteine at the indicated positions. A non-EGFR binding control

affibody Z domain containing a cysteine at position Q32 is also shown (Z-Q32). The mass range is cropped to a set of peaks corresponding to all peptides having net charge of +7. The most prominent peak in each spectrum corresponds to the mass of each mutant conjugated with maleimide-benzophenone. Results are shown in gel format above and as spectra below.

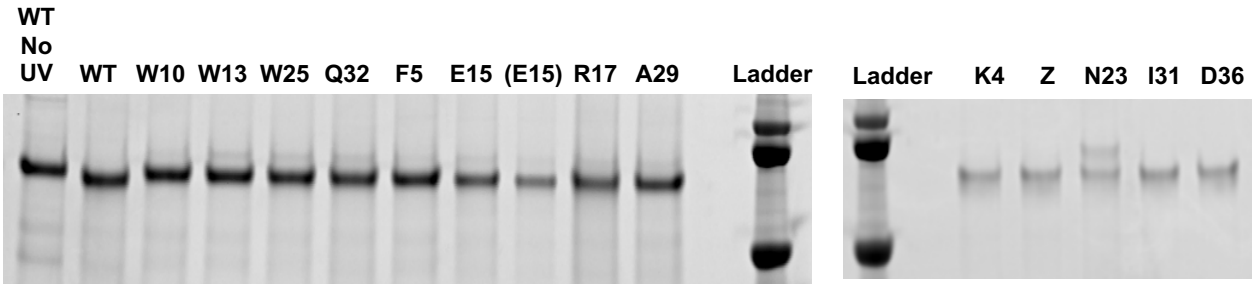

Figure S2: SDS-PAGE gels showing photocrosslinking of pure EGFR to various EGFR1907 affibodies mutated with cysteine at the indicated position. Z indicates the non-EGFR binding affibody parent protein containing a Q32C mutation. Affibody final concentration in all cases was 33 μM. EGFR final concentration was 0.53 μM for gel on left and 0.26 μM for gel on right.

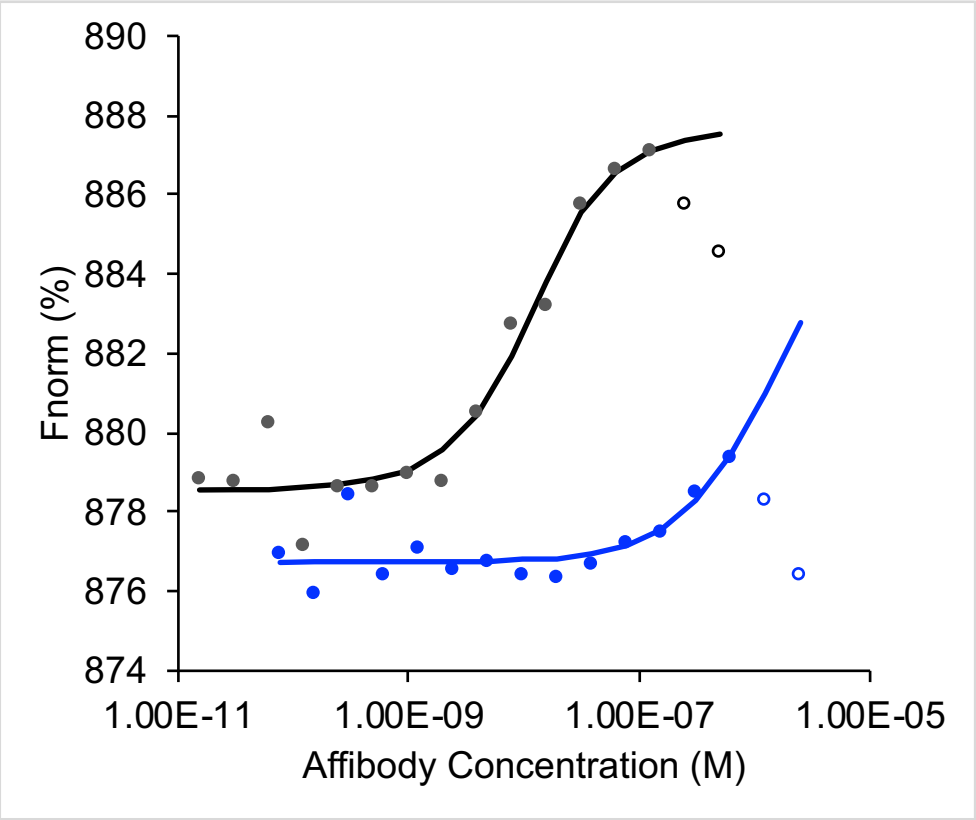

Figure S3: Comparison of microscale thermophoresis signals vs. affibody concentrations for both N23BP (blue) and WT (black) affibodies binding to 10 nM purified EGFR extracellular domain labeled with Alexa Fluor 647. The data were fitted with a quadratic binding equation and the fits for each data set are shown in matching colors. Data shown as hollow circles were excluded due to the formation of aggregates clearly visible in the MST traces at high concentrations of affibody.

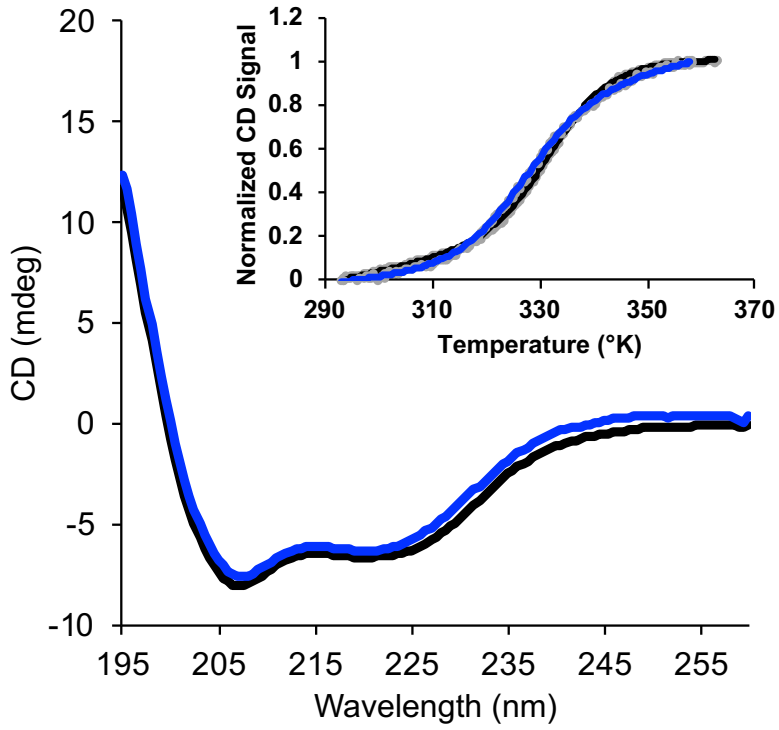

Figure S4: Overlay of circular dichroism spectra of N23BP (blue) and WT (black) as shown in Figure 3 in main text. Inset: Thermal denaturing curves of N23BP (blue) and WT (black) monitored at 222 nm. A small difference in melting temperatures was observed between N23BP and WT affibody (327.5±0.4 K vs 332.5±1.3 K, respectively).

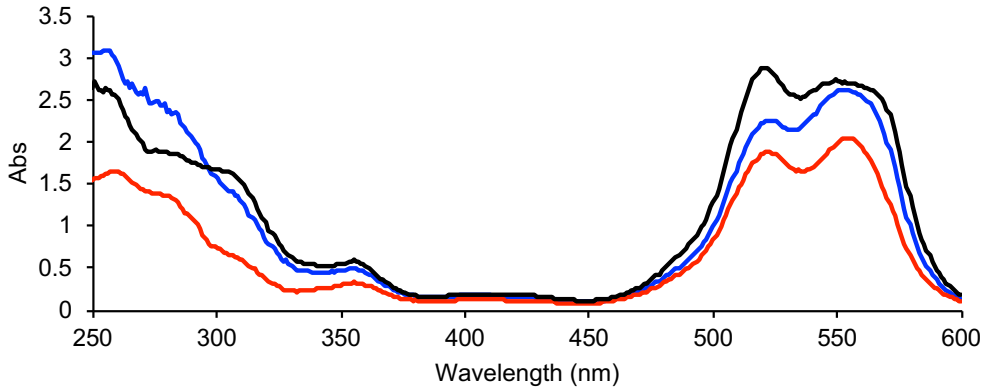

Figure S5: Absorbance spectra for photocrosslinkable affibody N23BP (blue) and two controls (WT, red; and Z, black) after conjugation with 5x molar excess Rhodamine-NHS.

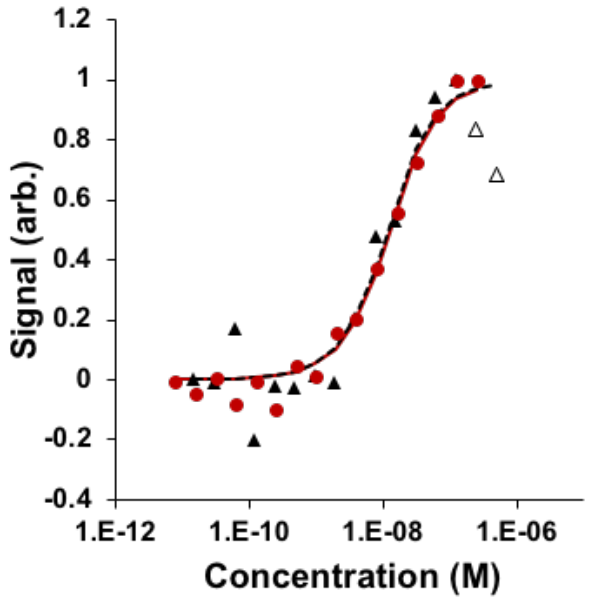

Figure S6: Overlaid microscale thermophoresis (MST) spectra of WT affibody with (red circles and solid line) and without (black triangles and dotted line) rhodamine conjugation. Empty triangles are auto-rejected data. The measured values, 7.13 ± 3.50 nM for WT and 7.99 ± 1.553 nM for Rh-WT, were not statistically different.

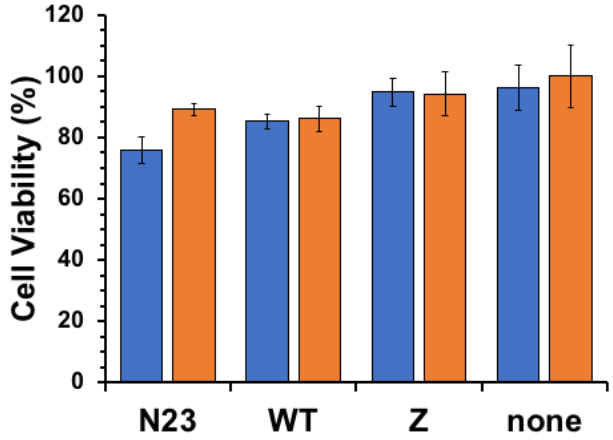

Figure S7: MTT assay showing the effects of affibody and UV irradiation on 4T1 cell viability. Left bar is with UV exposure as described in text, right bar is without UV exposure. Error bars are standard deviations from three replicates.

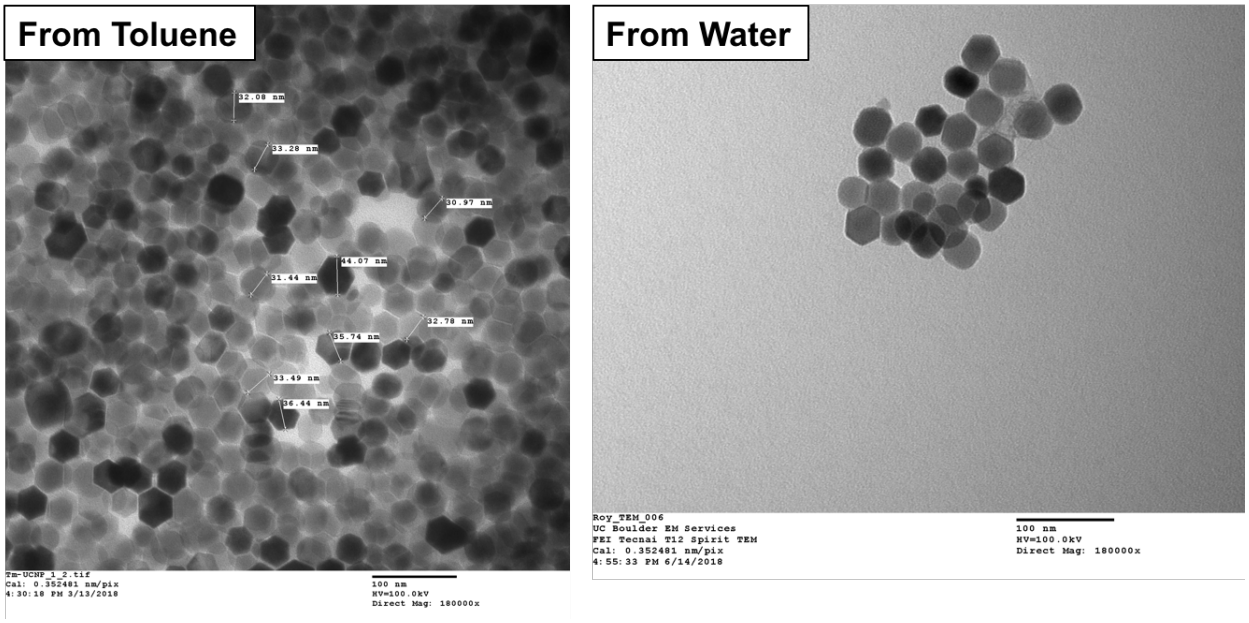

Figure S8: Left, center: Transmission Electron Micrograph of UCNPs deposited from toluene as-made (left) and from water (right) as stabilized by C18-PEG-NH_2.

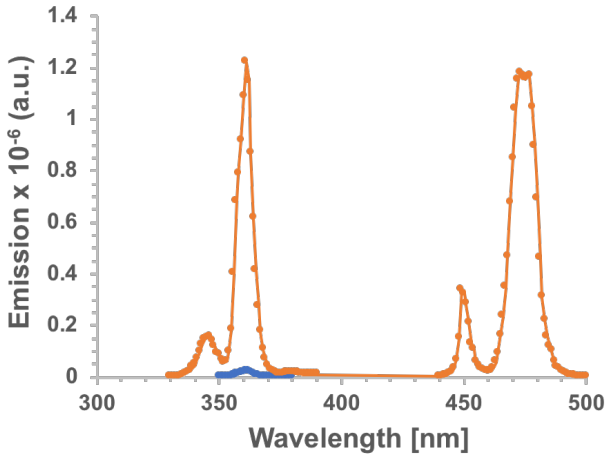

Figure S9: Emission spectra of UCNPs excited with 980 nm laser light (red), overlaid with absorption spectrum of a toluene blank (blue).